Supporting Information:

Nanodroplets at Membranes Create Tight-Lipped Membrane Necks *via* Negative Line Tension

Vahid Satarifard, Andrea Grafmüller, and Reinhard Lipowsky*

Theory & Biosystems, Max Planck Institute of Colloids and Interfaces, 14424 Potsdam, Germany

November 3, 2018

S1. Phase separation in binary AB mixture

The binary mixture of liquid-A and liquid-B beads provides a relatively simple model system that undergoes phase separation into two aqueous phases, the A-rich phase α and the B-rich phase β. In Figure S1, we describe the simulation geometries used to determine the interfacial tension $\Sigma_{\alpha\beta}$ and the two-phase coexistence region.

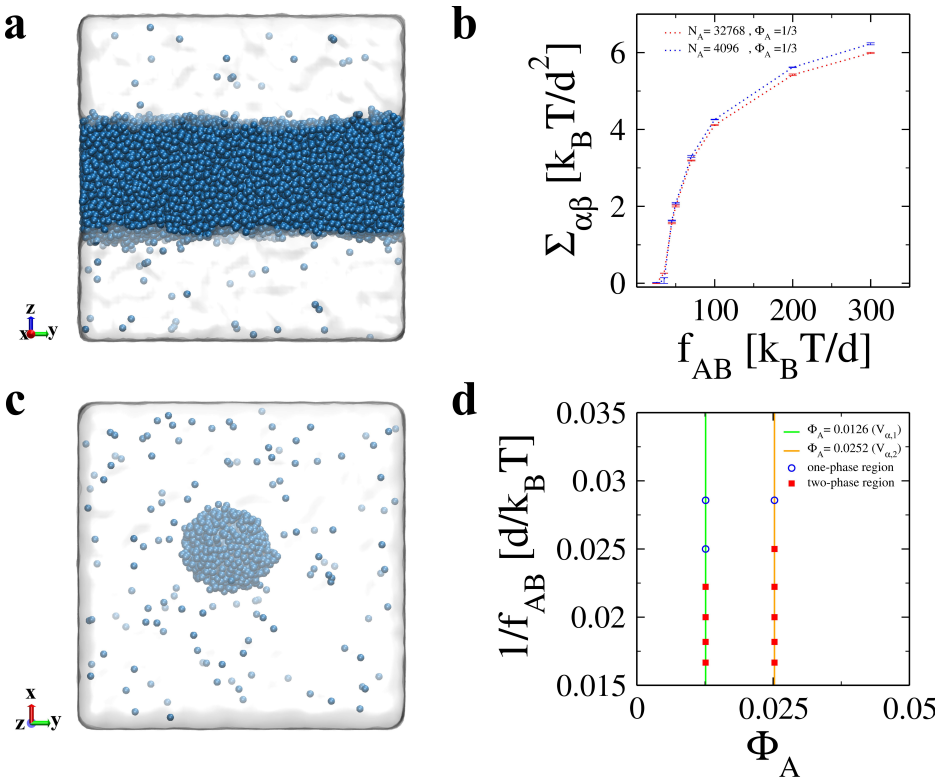

Figure S1: Two-phase coexistence and interfacial tension in a binary mixture of A and B water beads: (a) Two planar $\alpha\beta$ interfaces between the A-rich α phase (cyan) and the B-rich β phase (white). This slab geometry is convenient to measure the interfacial tension $\Sigma_{\alpha\beta}$ via the stress profile; (b) The interfacial tension $\Sigma_{\alpha\beta}$ as a function of the force parameter $f_{\rm AB}$ for constant force parameters $f_{\rm AA} = f_{\rm BB} = 25$; (c) Small droplet of α phase immersed in the β phase. The stability of such an α droplet provides a simple criterion for the coexistence of α and β; and (d) Depending on the mole fraction $\Phi_{\rm A}$ of the A beads and on the effective temperature $1/f_{\rm AB}$, small droplets of α phase remain stable (solid squares, red) or dissolve (open circles, blue). The left and right vertical line corresponds to the smaller volume $V_{\alpha,1}$ and to the larger volume $V_{\alpha,2} = 2V_{\alpha,1}$, respectively.

S2. Contact area and interfacial area of nanodroplet

During the time-dependent engulfment of the nanodroplet as displayed in Figure 2 and Movie1, corresponding to the parameter set DPD-1 in Table 1, the contact area $A_{\alpha\gamma}$ of the droplet with the membrane increases and the area $A_{\alpha\beta}$ of the water-water interface decreases. The precise evolution of these two areas is displayed in Figure S2 as a function of the lateral box size $L_{\parallel}$.

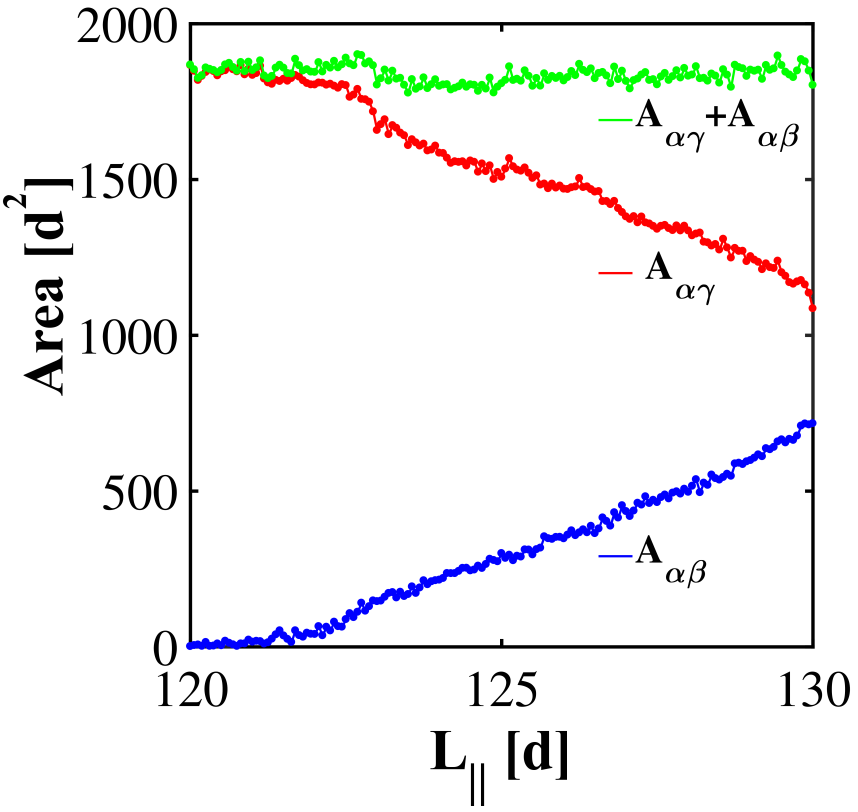

Figure S2: Dependence of the contact area $A_{\alpha\gamma}$ (red data) and interfacial area $A_{\alpha\beta}$ (blue data) of the nanodroplet on the lateral size $L_{\parallel}$ of the simulation box which is reduced from $L_{\parallel} = 130\,d$ at time $t = 0$ to $L_{\parallel} = 120\,d$ at time $t = 4\mu$s, compare Figure 2 and Movie1, where the bead diameter d is of the order of one nanometer and provides the basic length scale. During this reduction of $L_{\parallel}$, the interfacial area $A_{\alpha\beta}$ goes to zero because the membrane forms a closed neck that replaces the $\alpha\beta$ interface. For comparison, we also include the combined area $A_{\alpha\gamma} + A_{\alpha\beta}$ (green data) which represents the surface area of the droplet and stays essentially constant for all $L_{\parallel}$-values. Therefore, apart from the tight-lipped neck, the nanodroplet has an essentially spherical shape.

S3. Numerical results for symmetric bilayers with DPD-1 parameters

Table S1: Mechanical properties of the symmetric bilayers obtained for the parameter DPD-1 in Table 1 and volume $V_{\alpha,1} = 6837.6\ d^3$ of the α droplet. Lateral box size $L_\parallel$, interfacial tension $\Sigma_{\alpha\beta}$, mechanical tensions $\Sigma_{\alpha\gamma}$ and $\Sigma_{\beta\gamma}$ of the two membrane segments, and line tension $\lambda_{\alpha\beta\gamma}$ of the contact line.

	$L_\parallel[d]$	$\Sigma_{\alpha\beta}[k_BT/d^2]$	$\Sigma_{\alpha\gamma}[k_BT/d^2]$	$\Sigma_{\beta\gamma}[k_BT/d^2]$	$\lambda_{\alpha\beta\gamma}[k_BT/d]$
$V_{\alpha,1}$	130	1.861 ± 0.19	1.404 ± 0.18	0.854 ± 0.07	-7.305 ± 5.46
	135	1.913 ± 0.19	2.793 ± 0.27	2.193 ± 0.10	-8.430 ± 4.75
	140	1.889 ± 0.13	4.771 ± 0.19	4.184 ± 0.05	-10.008 ± 3.89
	145	1.852 ± 0.25	6.634 ± 0.20	6.141 ± 0.06	-11.402 ± 3.29
	150	1.952 ± 0.16	8.430 ± 0.17	7.842 ± 0.05	-12.203 ± 2.65

Table S2: Mechanical properties of symmetric DPD-1 bilayers for larger α droplet with volume $V_{\alpha,2} = 2V_{\alpha,1} = 13675.3\ d^3$. Lateral box size $L_\parallel$, interfacial tension $\Sigma_{\alpha\beta}$, mechanical tensions $\Sigma_{\alpha\gamma}$ and $\Sigma_{\beta\gamma}$ of the two membrane segments, and line tension $\lambda_{\alpha\beta\gamma}$.

	$L_\parallel[d]$	$\Sigma_{\alpha\beta}[k_BT/d^2]$	$\Sigma_{\alpha\gamma}[k_BT/d^2]$	$\Sigma_{\beta\gamma}[k_BT/d^2]$	$\lambda_{\alpha\beta\gamma}[k_BT/d]$
$V_{\alpha,2}$	135	1.959 ± 0.17	2.804 ± 0.21	2.272 ± 0.08	-9.110 ± 4.59
	140	1.891 ± 0.17	4.657 ± 0.15	4.229 ± 0.05	-10.122 ± 4.01
	145	1.982 ± 0.19	6.559 ± 0.23	6.160 ± 0.06	-11.748 ± 4.46
	150	1.928 ± 0.13	8.331 ± 0.23	7.854 ± 0.05	-12.302 ± 4.36

Table S3: Geometric properties of symmetric DPD-1 bilayers for smaller α droplet with volume $V_{\alpha,1} = 6837.6\ d^3$. Lateral box size $L_\parallel$, corresponding segment tension $\Sigma_{\beta\gamma}$ in units of k_BT/d^2 as in Table S1, base area $A_\parallel = L_\parallel^2$, intrinsic contact angle θ_α^*, contact line radius R_{co}, and cosine of tilt angle, $\cos\psi_{co}$, at contact line.

	$L_\parallel[d]$	$\Sigma_{\beta\gamma}$	$A_\parallel[d^2]$	θ_α^*[degree]	$R_{co}[d]$	$\cos\psi_{co}$
$V_{\alpha,1}$	130	0.854	16900	96.984 ± 2.63	13.75 ± 0.09	0.6 ± 0.03
	135	2.193	18225	92.988 ± 2.19	14.24 ± 0.06	0.83 ± 0.03
	140	4.184	19600	88.184 ± 2.88	14.38 ± 0.19	0.92 ± 0.02
	145	6.141	21025	81.058 ± 1.74	14.22 ± 0.03	0.98 ± 0.01
	150	7.842	22500	83.100 ± 1.80	14.14 ± 0.06	0.95 ± 0.01

Table S4: Geometric properties of symmetric DPD-1 bilayers for larger α droplet with volume $V_{\alpha,2} = 2V_{\alpha,1} = 13675.3\ d^3$. Lateral box size $L_\parallel$, corresponding segment tension $\Sigma_{\beta\gamma}$ in units of k_BT/d^2 as in Table S2, base area $A_\parallel = L_\parallel^2$, intrinsic contact angle θ_α^*, contact line radius R_{co}, and cosine of tilt angle, $\cos\psi_{co}$, at contact line.

	$L_\parallel[d]$	$\Sigma_{\beta\gamma}$	$A_\parallel[d^2]$	θ_α^*[degree]	$R_{co}[d]$	$\cos\psi_{co}$
$V_{\alpha,2}$	135	2.272	18225	93.059 ± 3.55	18.59 ± 0.06	0.87 ± 0.04
	140	4.229	19600	87.288 ± 3.13	18.48 ± 0.06	0.93 ± 0.02
	145	6.160	21025	83.744 ± 2.73	18.32 ± 0.05	0.96 ± 0.01
	150	7.854	22500	85.116 ± 1.72	18.43 ± 0.06	0.96 ± 0.01

S4. Different contributions to total free energy

As explained in the *Methods* section of the main text, see eq 4, the total free energy of the membrane-droplet system can be decomposed into separate contributions, corresponding to the interfacial free energy $\Sigma_{\alpha\beta}A_{\alpha\beta}$ of the $\alpha\beta$ interface, the bending energy $E_{\rm be}$ of the membrane, and the line free energy $\lambda_{\alpha\beta\gamma}L_{\alpha\beta\gamma}$ of the contact line. These different free energy contributions are displayed in Figure S3 for two values of the lateral box size $L_\parallel$. The data in Figure S3a,b are also included in Movie2.

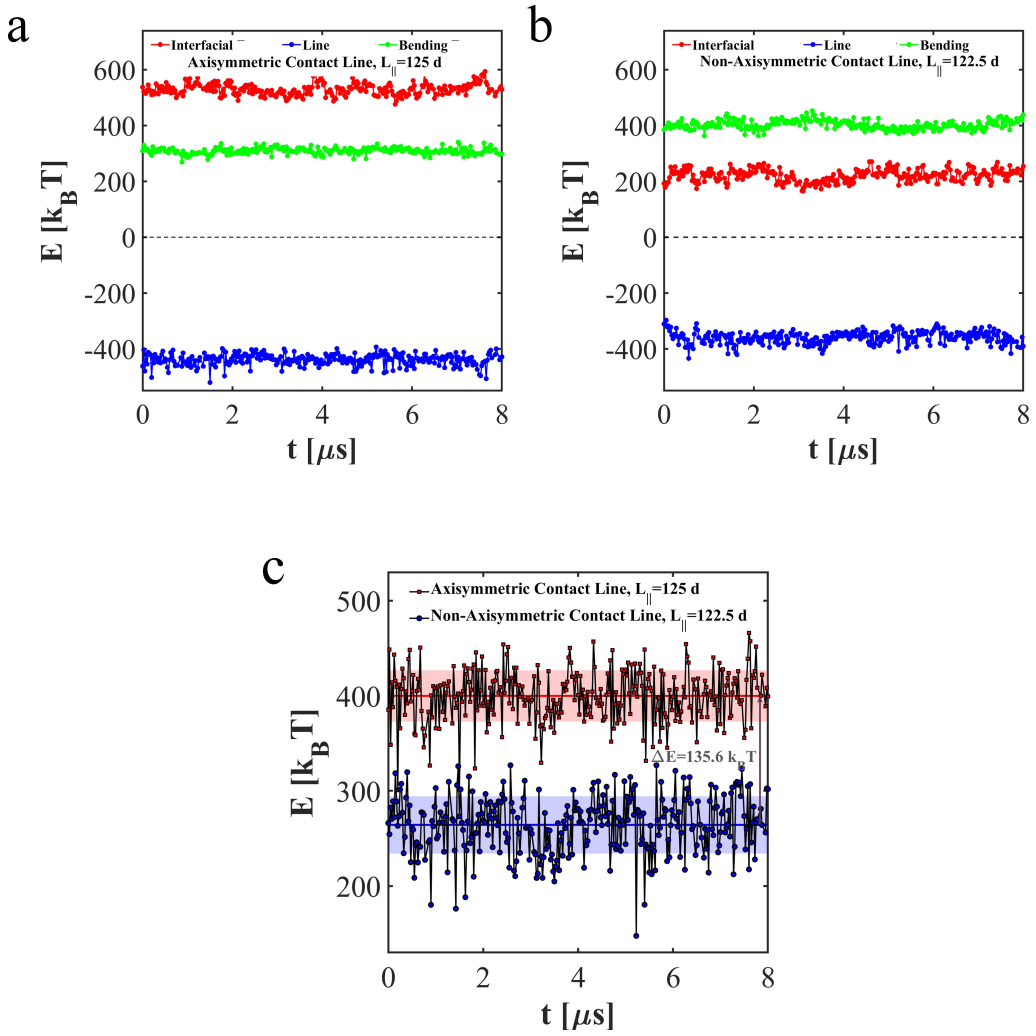

Figure S3: (a,b) Positive interfacial free energy (red), positive bending energy (green), and negative line free energy (blue) as a function of time t for two values of the lateral box size $L_\parallel$: (a) For $L_\parallel = 125\,d$, the membrane-droplet system is axisymmetric with a circular contact line; (b) For the slightly smaller value $L_\parallel = 122.5\,d$, the axisymmetry is broken and the contact line has an elongated, noncircular shape. During the transition from (a) to (b), the interfacial free energy is strongly reduced, the bending energy is slightly increased, and the line free energy remains almost constant; and (c) Total free energy E for the axisymmetric morphology with $L_\parallel = 125\,d$ (top) and for the non-axisymmetric morphology with $L_\parallel = 122.5\,d$ (bottom). Thus, during the morphological transition from the axisymmetric to the non-axisymmetric shape, the total free energy is reduced by $\Delta E = 135.6\,k_{\rm B}T$.

S.5 Numerical computation of bending energies

To calculate the bending energies, we use the following numerical protocol. For a given bead configuration, as obtained from the DPD simulations, we first construct the midsurface of the bilayer membrane, from the positions of the lipid head beads in the two leaflets, and triangulate this surface using a Delaunay scheme. For each vertex i of the Delaunay triangulation, we consider the K_i triangles (or faces) adjacent to vertex i, i.e., those triangles for which vertex i represents one corner, and label these triangles by $k_i = 1, \ldots, K_i$. Each triangle k_i has the area $A(k_i)$. The effective vertex area is then defined by

$$A_i \equiv \frac{1}{3} \sum_{k_i=1}^{K_i} A(k_i) \tag{S1}$$

where the sum runs over all triangles adjacent to vertex i. The factor $1/3$ takes into account that three vertices share one triangle and ensures that the total area of the midsurface is given by $\sum_i A_i$, i.e., by the sum over the effective vertex areas. The mean curvature M_i associated with vertex i is computed using the algorithm introduced in Ref. [1]. For a symmetric bilayer with zero spontaneous curvature and bending rigidity κ, the discretized bending energy is then given by

$$E_{\rm be}^{\rm dis}\{A_i, M_i\} = 2\kappa \sum_i A_i M_i^2 \tag{S2}$$

where the sum runs over all vertices of the triangulation. For the parameter set DPD-1, the bending rigidity κ has the value $\kappa \simeq 12.6\, k_{\rm B}T$, which was calculated from the area compressibility modulus as in Refs. [2] and [3].

When we insert the effective vertex areas $A_i^{(0)}$ and the mean curvatures $M_i^{(0)}$ of the original Delaunay triangulation into eq S2, we obtain the bending energy $E_{\rm be}^{(0)} \equiv E_{\rm be}^{\rm dis}\{A_i^{(0)}, M_i^{(0)}\}$. We then start to smoothen the small-scale roughness of the bilayer membrane by applying the mean face normal filter developed in Ref. [4] to the triangulated midsurface. For this smoothened surface, we again compute the effective vertex areas $A_i^{(1)}$ and the vertex-associated mean curvatures $M_i^{(1)}$ to obtain the bending energy $E_{\rm be}^{(1)} = E_{\rm be}^{\rm dis}\{A_i^{(1)}, M_i^{(1)}\}$. The smoothening and the associated computation are iterated several times, thereby generating a series of bending energy values $E_{\rm be}^{(n)}$. The iterative smoothening is stopped when the change in the bending energy falls below $1\, k_{\rm B}T$, i.e., it is stopped at $n = N$ with $|E_{\rm be}^{(N)} - E_{\rm be}^{(N-1)}| < k_{\rm B}T$.

The numerical procedure just described was used to calculate the bending energies shown in Figure S3 and Movie2. When we apply the same procedure to the membrane in Figure 2d, which exhibits a tight-lipped membrane neck, we obtain the bending energy $E_{\rm be}^{(N)} = 438.5\, k_{\rm B}T$ after $N = 61$ smoothening iterations. To compute the excess bending energy of the neck, we substract the bending energy $8\pi\kappa$ of a spherical $\alpha\gamma$ membrane segment and take into account that the bending energy of a planar $\beta\gamma$ membrane segment vanishes. For the bending rigidity $\kappa = 12.6\, k_{\rm B}T$, we then obtain the bending energy

$$\Delta E_{\rm be} = E_{\rm be}^{(N)} - 8\pi\kappa = 438.5\, k_{\rm B}T - 316.7\, k_{\rm B}T = 121.8\, k_{\rm B}T\,. \tag{S3}$$

Using the length $L_{\alpha\beta\gamma} \simeq 70\, d$ of the contact line in Figure 2d, we obtain the contribution $\Delta E_{\rm be}/L_{\alpha\beta\gamma} \simeq 1.74\, k_{\rm B}T/d$ to the effective line tension $\lambda_{\rm eff}$ from the highly curved membrane segments along the contact line.

S.6 Affinity contrast and spontaneous curvature

The interactions of the lipid head (H) beads with the A and B water beads are described by the DPD force parameters $f_{\rm AH}$ and $f_{\rm BH}$. If $f_{\rm BH} > f_{\rm AH}$, the H beads prefer to be in contact with the A beads; if $f_{\rm AH} > f_{\rm BH}$, the H beads prefer the B beads. The corresponding affinity contrast $\Delta_{\rm aff}$ was defined in Eq 2 of the main text and is given by

$$\Delta_{\rm aff} = \frac{f_{\rm BH} - f_{\rm AH}}{f_{\rm BH}} \,. \tag{S4}$$

As explained in the main text, a nonzero affinity contrast generates a nonzero spontaneous curvature m, which can be positive or negative. In order to uniquely define the sign of this curvature, we use two conventions. First, we define m to be negative if the bilayer prefers to bend (or bulge) towards the inner leaflet and the interior aqueous solution. Second, we consider the spectator phase γ to represent the interior solution. Thus, the spontaneous curvature $m_{\alpha\gamma}$ is *negative* if the $\alpha\gamma$ bilayer segment prefers to bulge towards the spectator phase γ and positive otherwise.

To determine the spontaneous curvature m arising from a nonzero affinity contrast, we used the parameter set DPD-3 as given in Table 3 of the main text. Apart from $f_{\rm AH}$, all force parameters have the same values as for the parameter set DPD-1. The force parameter $f_{\rm AH}$ between the A water beads and the lipid head beads was taken to be 22.5 and 27.5 $k_{\rm B}T/d$ in addition to the value $f_{\rm AH} = f_{\rm BH} = 25\, k_{\rm B}T/d$ for a symmetric bilayer. For fixed force parameter $f_{\rm BH} = 25\, k_{\rm B}T/d$, the three $f_{\rm AH}$-values 22.5, 25, and 27.5 $k_{\rm B}T/d$ correspond to the affinity contrasts $\Delta_{\rm aff} = 0.1, 0$, and -0.1.

In order to determine the spontaneous curvature $m_{\alpha\gamma}$ associated with this bilayer asymmetry, we used the protocol developed in Ref. [5]. We considered two planar bilayers spanning the simulation box, both exposed to the α and γ phases as in Figure S4, and calculated the stress profile $S_{\alpha\gamma}$ across both bilayers as shown in Figure S5a1-c1. We then divide the stress profile $S_{\alpha\gamma}$ up into two stress profiles, $S_{z<0}$ and $S_{z>0}$, across the two individual bilayers. The first moments of these individual stress profiles are related to the spontaneous curvature $m_{\alpha\gamma}$ via

$$\int_{-25d}^{0} {\rm d}z\, S_{z<0}(z) z = \int_{25d}^{0} {\rm d}z\, S_{z>0}(z) z = -2\kappa m_{\alpha\gamma} \tag{S5}$$

from which we can deduce the spontaneous curvature $m_{\alpha\gamma}$ using the bending rigidity $\kappa = 12.6\, k_{\rm B}T$.

References

[1] Dirk Jan Kroon. Patch Curvature. *http://uk.mathworks.com/matlabcentral/fileexchange/32573-patch-curvature.*, 2014.

[2] R. Goetz, G. Gompper, and R. Lipowsky. Mobilitiy and Elasticity of Self-Assembled Membranes. *Phys. Rev. Lett.*, 82:221–224, 1999.

[3] A. Sreekumari and R. Lipowsky. Lipids with Bulky Head Groups Generate Large Membrane Curvatures by Small Compositional Asymmetries. *J. Chem. Phys.*, 149:084901, 2018.

[4] Hirokazu Yagou, Yutaka Ohtake, and Alexander Belyaev. Mesh Smoothing via Mean and Median Filtering Applied to Face Normals. In *null*, page 124. IEEE, 2002.

[5] Bartosz Różycki and Reinhard Lipowsky. Spontaneous Curvature of Bilayer Membranes from Molecular Simulations: Asymmetric Lipid Densities and Asymmetric Adsorption. *J. Chem. Phys.*, 142(5):02B601_1, 2015.

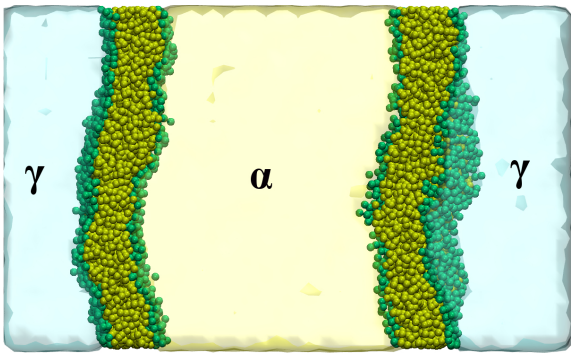

Figure S4: Simulation snapshot of the two planar bilayers used to measure the spontaneous curvature $m_{\alpha\gamma}$ of the $\alpha\gamma$ membrane segment. Both bilayers are in contact with the A-rich phase α (yellow) and the liquid phase γ which consists only of B beads (light blue) over the time scale of our simulations, see Figure S5a2-c2.

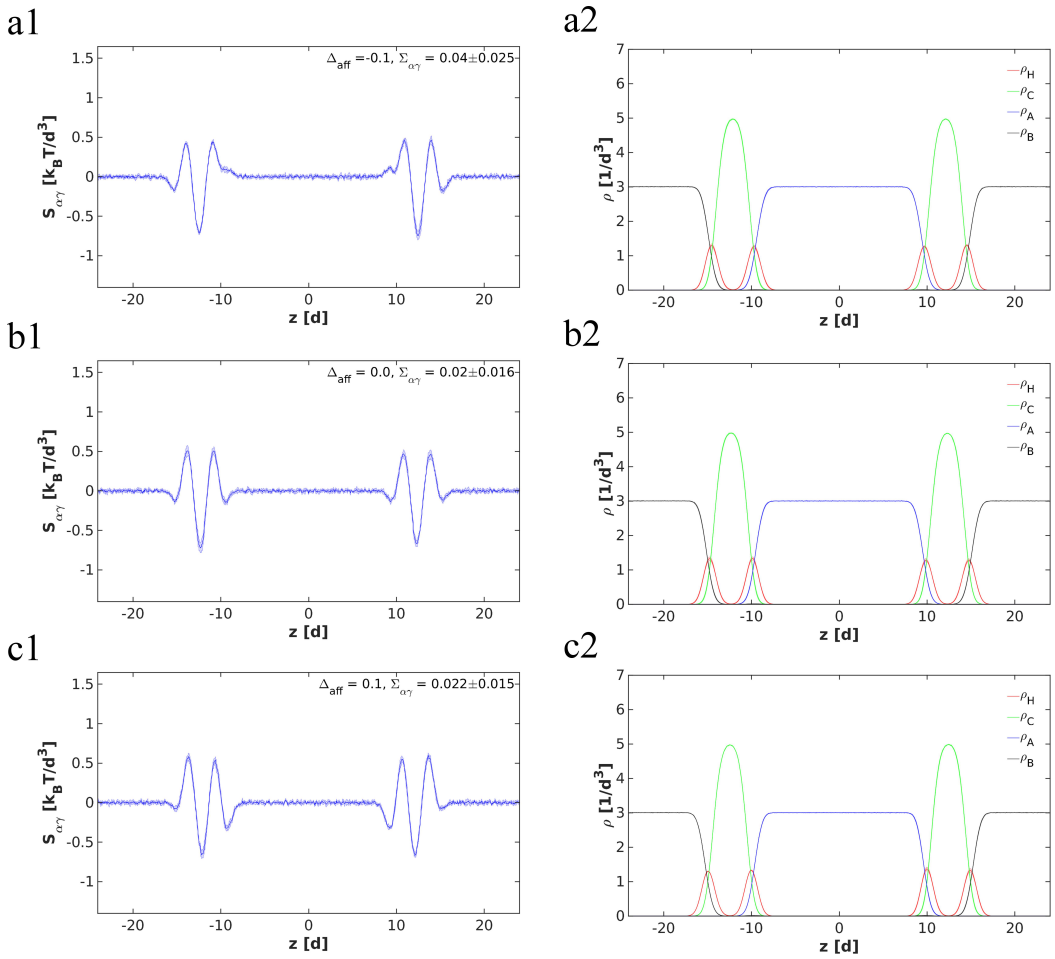

Figure S5: (a1 - c1) Stress profiles $S_{\alpha\gamma}$ and (a2 - c2) bead density profiles ρ as functions of the coordinate z perpendicular to the two bilayers in Figure S3. The profiles in (a1) and (a2) correspond to the affinity contrast $\Delta_{\text{aff}} = 0.1$, the profiles in (b1) and (b2) to a symmetric membrane with $\Delta_{\text{aff}} = 0$, and those in (c1) and (c2) to $\Delta_{\text{aff}} = -0.1$. Using the relation in eq S5 with the bending rigidity $\kappa = 12.6\, k_{\text{B}}T$, we obtain the spontaneous curvatures $m = 0.047/d, 0.003/d$, and $-0.044/d$ for $\Delta_{\text{aff}} = 0.1, 0$, and -0.1, respectively.

Movie Captions

Movie1. Time-dependent engulfment of nanodroplet (dark blue) by lipid bilayer (green chains, yellow heads), viewed from the bottom and via two orthogonal cross-sections: The membrane tension is controlled by the lateral size $L_\parallel$ of the simulation box which is reduced, for fixed number of lipid molecules, from $L_\parallel = 130\,d$ at $t = 0$ to $L_\parallel = 120\,d$ at $t = 4\,\mu$s, with the basic length scale provided by the bead diameter d which is of the order of 1 nm. At $t = 0$, the droplet adheres to the bilayer membrane and is partially engulfed by it. As we reduce the box size $L_\parallel$ and thus the membrane tension with constant velocity $\mathrm{d}L_\parallel/\mathrm{d}t$, the contact area of the droplet with the membrane increases while the area of the $\alpha\beta$ interface decreases, see also Figure S1. The rotational symmetry of the membrane-droplet morphology is spontaneously broken at $L_\parallel = L_\parallel^* \simeq 124\,d$. For $L_\parallel < L_\parallel^*$, the morphology is characterized by a noncircular contact line and an elongated membrane neck. This non-axisymmetric morphology persists until the membrane neck closes, thereby attaining a tight-lipped shape. In Figure 2 of the main text, we display four snapshots of this movie.

Movie2. Shape and energy fluctuations of the nanodroplet (dark blue) partially engulfed by the bilayer membrane (green chains, yellow head groups), for two lateral box sizes $L_\parallel$ close to the morphological transition at $L_\parallel^* \simeq 124\,d$: (Top row) For fixed box size $L_\parallel = 125\,d > L_\parallel^*$, the membrane-droplet morphology is, on average, axisymmetric; and (Bottom row) For box size $L_\parallel = 122.5\,d < L_\parallel^*$, the morphology is non-axisymmetric. In both cases, the free energy of the $\alpha\beta$ interface (red) and the bending energy of the membrane (green) are positive whereas the free energy of the contact line (blue) is negative. As we decrease the box size from $L_\parallel = 125\,d$ to $L_\parallel = 122.5\,d$, the interfacial free energy decreases strongly, the bending energy increases significantly, and the line free energy stays almost constant. Summing up all three contributaions, we find that the total free energy is reduced by $135.6\,k_\mathrm{B}T$ as the box size is decreased from $L_\parallel = 125\,d$ to $L_\parallel = 122.5\,d$ and the membrane-droplet system undergoes a morphological transition from an axisymmetric to a non-axisymmetric shape.